Обзор ArXiv/astro-ph, 11-16 февраля 2026

От Сильченко О.К.

ArXiv: 2602.11783

Characterising Lyα damping wings at the onset of reionisation

Evidence for highly efficient star formation driven by dense, neutral gas in UV-bright galaxies at $z > 9$

Clara L. Pollock⋆[1,2], Kasper E. Heintz[3,1,2], Joris Witstok[1,2], Rashmi Gottumukkala[1,2], Gabriel Brammer[1,2], Sownak Bose[4], Alex J. Cameron[1,2], Pratika Dayal[5,6,7], Pieter van Dokkum[8], Johan Fynbo[1,2], Viola Gelli[1,2], Matthew J. Hayes[9], Akio K. Inoue[10,11], Claudia del P. Lagos[12,1], Peter Laursen[1,2], Romain A. Meyer[13], Rohan Naidu[14], Pascal Oesch[13,1,2], Lucie E. Rowland[15], Nial R. Tanvir[16], Sandro Tacchella[17,18], Chamilla Terp[1,2], Francesco Valentino[3,1], Fabian Walter[19], John Weaver[14], and Callum Witten[13]

Спектральная выборка JWST

- 48 галактик из разных площадок
- Призменные спектры JWST/NirSpec
- Z>9
- Причем красные смещения определяются независимо от Lya, по другим эмиссионным линиям
- Далее Lya моделируется суммой эмиссии и абсорбции

Определение колонковой плотности атомарного водорода

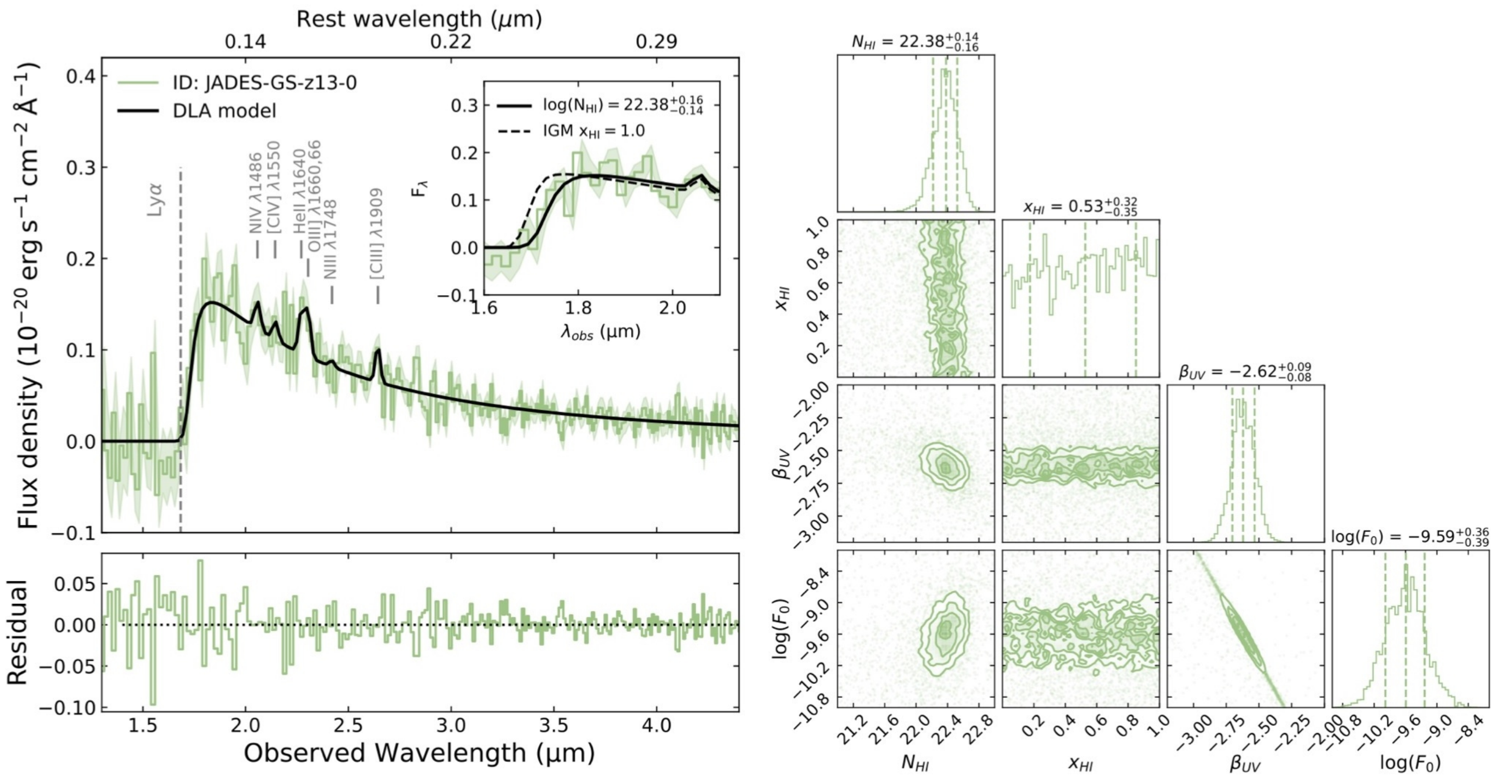

Fig. 1: *Left:* Example of UV emission line and DLA fitting for JADES-GS-z13-0 (DJA ID 3215_20128771) at $z = 12.85$. The NIRSpec/Prism spectrum and associated error are shown in green. The marked UV emission lines were modelled and then superimposed on the intrinsic spectrum before modelling the DLA (solid black line). In the inset, we show a zoom on the Lyα region, with the DLA+IGM model as a solid line, and with 100% neutral IGM only ($x_{HI} = 1.0$) as a dashed line. *Right:* Corner plot of the posterior distributions for the DLA+IGM model, with median, 16th and 84th percentiles marked.

Колонковая плотность водорода растет с красным смещением

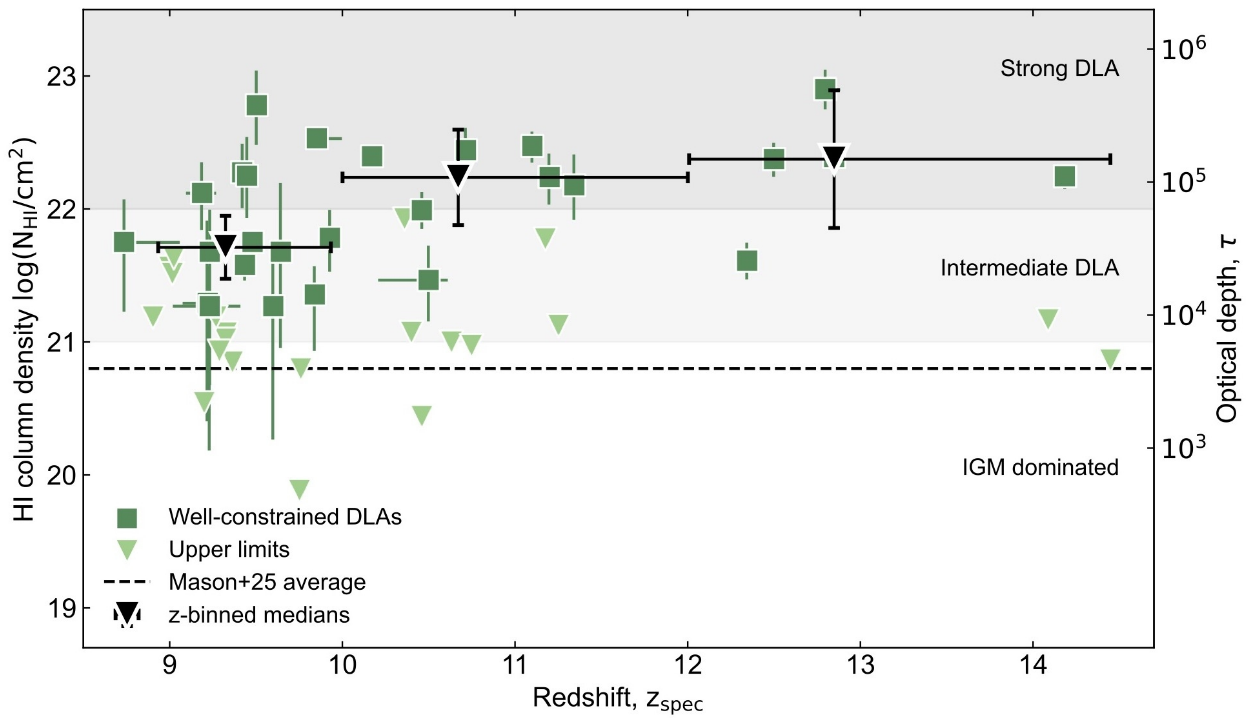

Fig. 2: Calculated column densities across the redshift range of the sample, dark green squares are well-constrained column densities with values $N_{\rm HI} > 10^{21}\,{\rm cm}^{-2}$. Upper limits are plotted as triangles, derived from the 95th percentile of the posterior distribution. The different shaded regions represent low column density ($N_{\rm HI} < 10^{21}\,{\rm cm}^{-2}$) where objects are likely IGM-dominated, high column densities ($N_{\rm HI} > 10^{21-22}\,{\rm cm}^{-2}$) where neutral hydrogen exceeds abundance from a fully neutral IGM, and very strong DLAs ($N_{\rm HI} > 10^{22}\,{\rm cm}^{-2}$) with an extreme over-abundance of neutral gas. Regardless of column density, all objects are optically thick with optical depths at the Lyman limit $\tau > 10^3$, with the highest column densities $N_{\rm HI} = 10^{22}\,{\rm cm}^{-2}$ corresponding to optical depths $\tau \approx 10^5$. Medians of well-constrained column density binned in redshift ($z < 10$, $10 < z < 12$, $z > 12$) are shown as black triangles (with values $N_{\rm HI} = 10^{21.71}, 10^{22.24}$, and $10^{22.37}\,{\rm cm}^{-2}$ respectively). These are essentially upper limits, as the fraction of IGM-dominated galaxies/upper limits (which were not included in the median) in each bin is 0.42, 0.50, and 0.29 respectively.

Сравнение с LCDM-предсказаниями

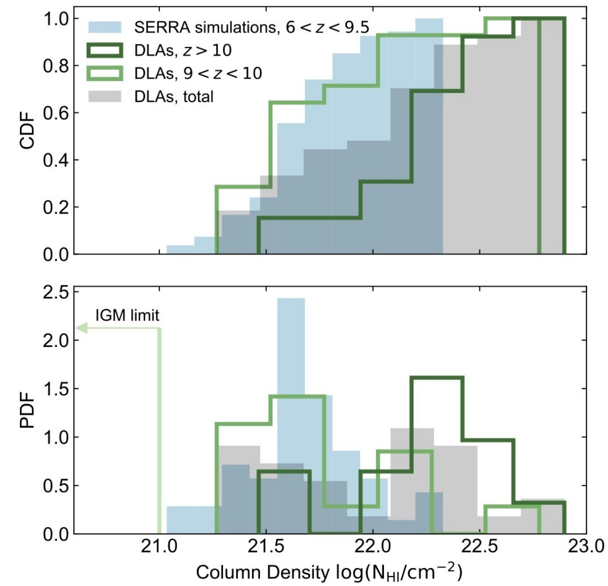

Fig. 4: *Top*: Cumulative histogram of derived column densities for our sample in shades of green; separated for non-DLAs (column densities < 10^{21} cm^{-2}), and the DLA sample (column densities > 10^{21} cm^{-2}) for $z = 9 - 10$ and $z > 10$. The full sample is shown as grey shaded region, comparing directly to the averages of *SERRA*-simulated galaxies $z = 6 - 9.5$ in blue (Gelli et al. 2025), showing that while the spread of observed DLAs is broadly consistent, there is a peak of extreme-DLAs (> 10^{22} cm^{-2}) that are not represented in the averages of simulations, particularly for those $z > 10$. *Bottom:* Similar to top panel, but for a normalised PDF, along with the fraction of galaxies with unconstrained DLAs shown as an IGM limit.

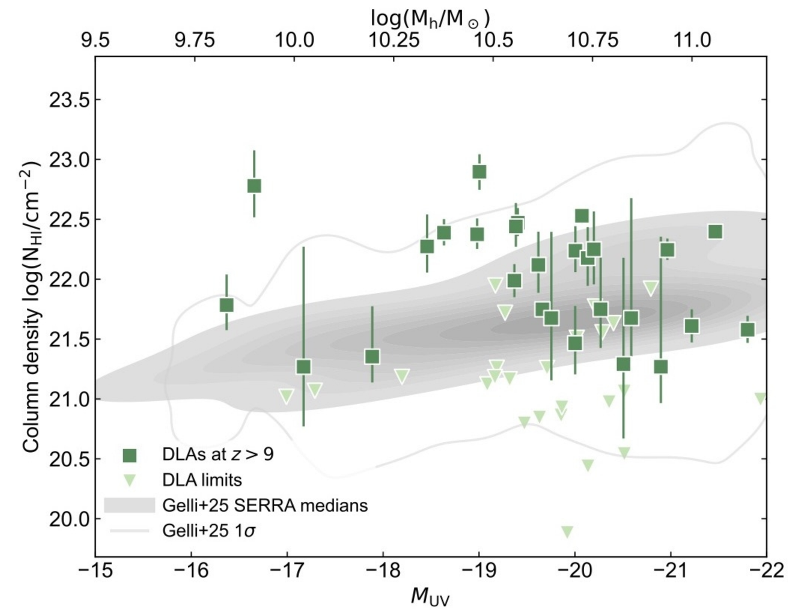

Fig. 5: Measured UV magnitude and column density. Halo masses for our objects are derived from UV magnitudes (Mason et al. 2023, no dust model). The well-constrained column densities of our sample are consistent with results from *SERRA* simulations (Gelli et al. 2025). The grey contours represent the average column density of 100 galaxies over random sight-lines, with the 1σ error region also shown, representing the scatter across sightlines in simulations.

Пыли таки мало

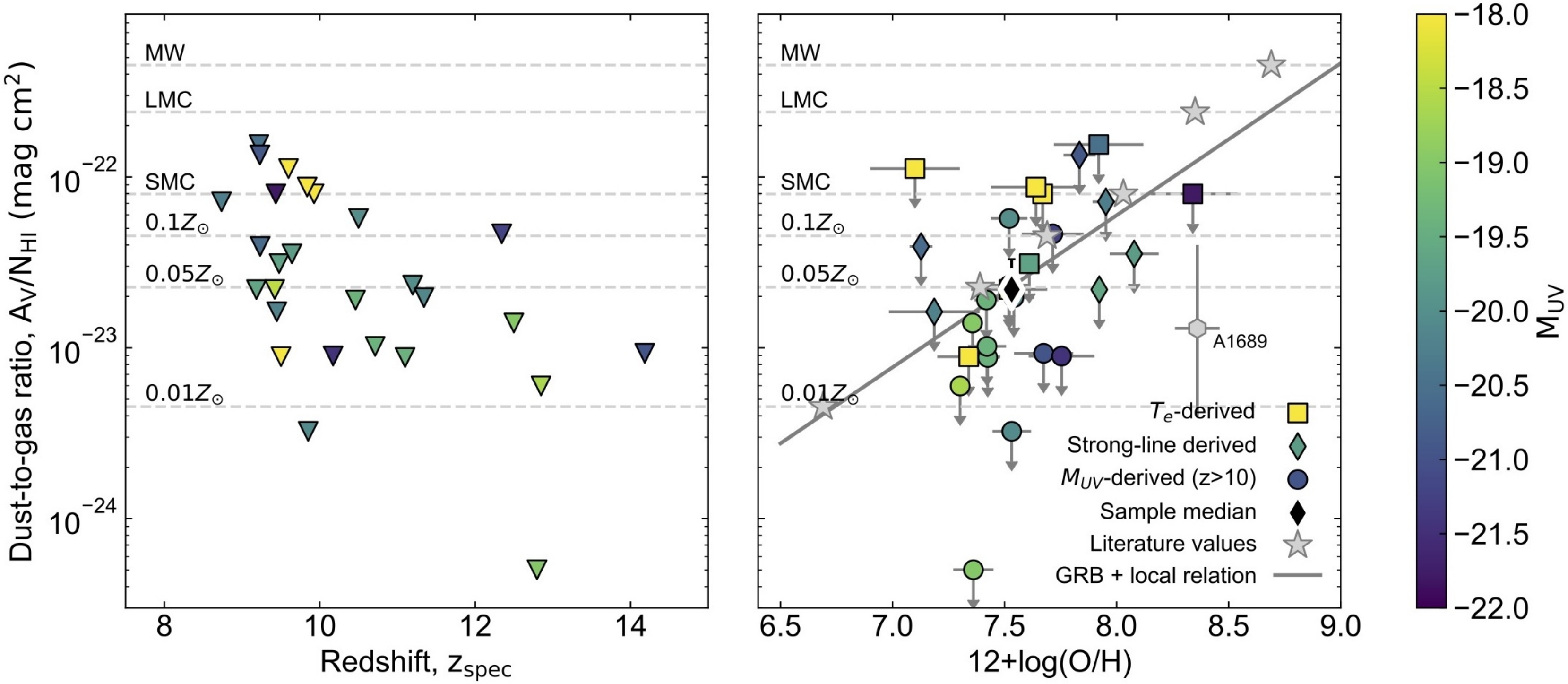

Fig. 6: *Left*: Upper limits for the dust-to-gas ratio $A_V/N_{\rm HI}$ against redshift, for the subsample of DLAs with $N_{\rm HI} > 10^{21}$ cm^{-2}. Here, A_V are derived from the assumed reddening of the β_{UV} slope, and so are taken to be upper limits. The majority of the sample are consistent with being dust-poor, lying below 10% solar metallicity. *Right*: The trend of $A_V/N_{\rm HI}$ against gas-phase metallicity 12+log(O/H), compared to values from the Milky Way, Large and Small Magellanic Clouds, and 10%, 5%, and 1% metallicities (metallicity for each represented with a star). The black line shows the relation for local galaxies and gamma-ray bursts (GRBs) (Heintz et al. 2023b). The method for calculating metallicity for each object is represented by different symbols; each still represents an upper limit in $A_V/N_{\rm HI}$, and is colour-coded with lensing-corrected UV magnitude.

Газ таки первичный

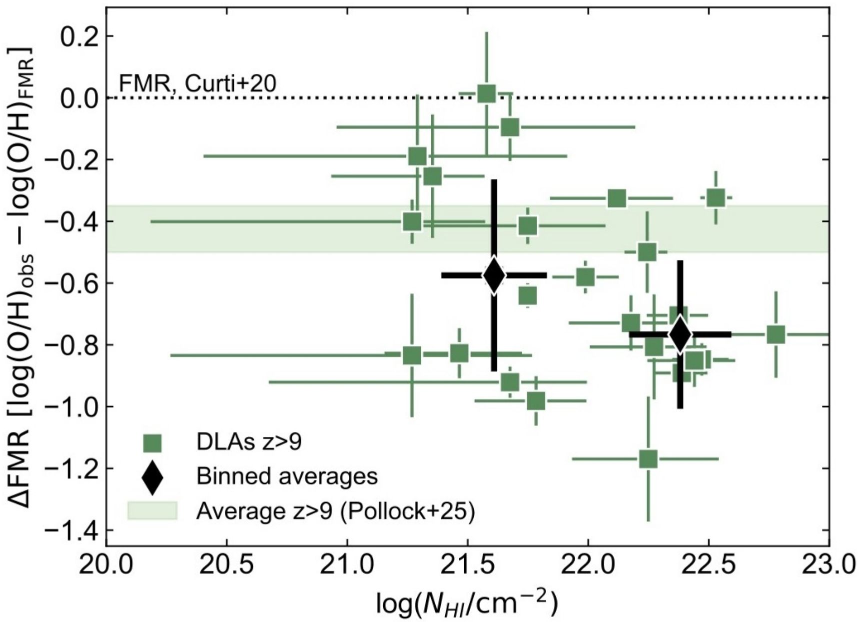

Fig. 7: Offset from the Fundamental Metallicity Relation (FMR, Curti et al. 2020) as a function of the H I column density for the sample of constrained DLAs. Binned averages for $N_{\rm HI} = 10^{21-22}$ cm^{-2} and $N_{\rm HI} > 10^{22}$ cm^{-2} are shown as black diamonds, with 1σ error bars. The average offset from metallicity measurements at $z = 9 - 10$ (Pollock et al. 2025) is shown in light green. There is only a moderate correlation, with Spearman rank $\rho \approx -0.4$, however the strongest DLAs tend to show large offsets from the FMR, as would be expected from pristine gas inflow dilution.

А вот эффективность звездообразования ОЧЕНЬ высока

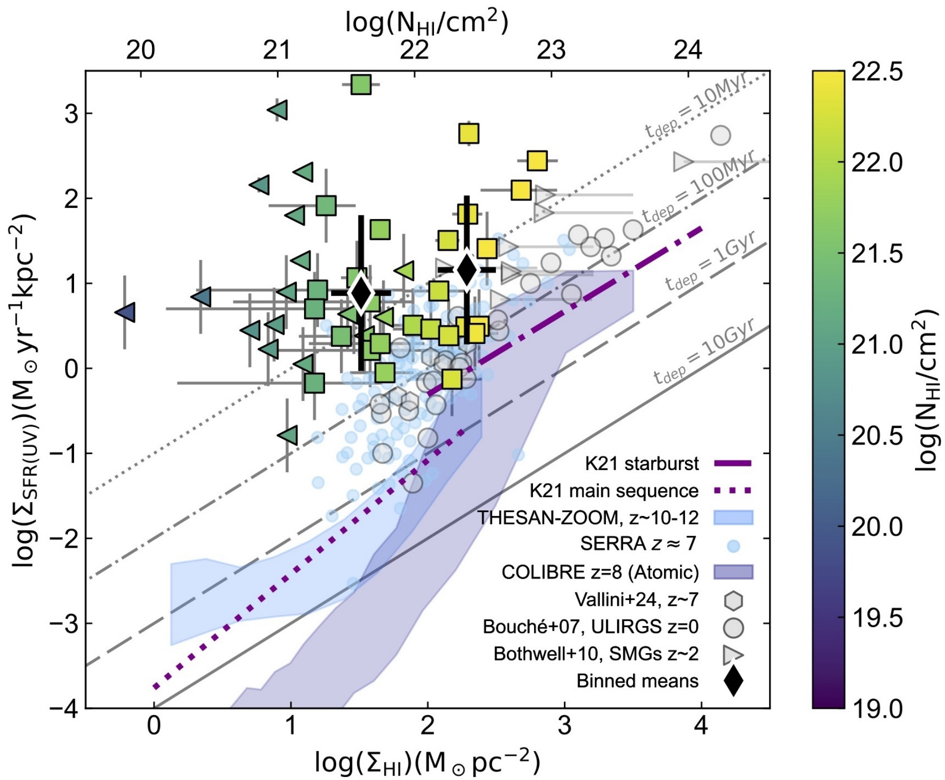

Fig. 8: Atomic Kennicutt-Schmidt relation of $\log(\Sigma_{\rm HI})$ and $\log(\Sigma_{\rm SFR})$, coloured with column density values. As previously, we plot non-constrained values as upper limits (95%). We compare to the canonical Kennicutt & De Los Reyes (2021) (K21) relations for starburst and main sequence galaxies, as well as various gas consumption depletion times corresponding to global star-formation efficiency in grey (Kennicutt 1998, $N = 1.0$). All galaxies lie above the empirical law, with some scatter, and the low column density (non-DLA) objects are extremely offset, even when plotted as upper limits. The binned means for $\Sigma_{\rm gas} = 10^1 - 10^2$, and $10^2 - 10^3\,{\rm M_\odot\,pc^{-2}}$ are shown as black diamonds, both consistent with $\sim 10\,$Myr. In shades of blue we compare to simulation predictions from *THESAN-ZOOM* at $z = 10-12$ (Shen et al. 2026; Kannan et al. 2025), *SERRA* at $z = 7$ (Pallottini et al. 2022), and H I-only gas surface density from *COLIBRE* at $z = 8$ (Lagos et al. 2025). Various literature measurements are shown in grey: from *ALMA* detections of [O III] 88μm and [C II] 158μm (Vallini et al. 2024) at $z \approx 7$, CO-based measurements for starburst ULIRGs at $z \sim 0$ (Bouché et al. 2007), and SMGs at $z \sim 2$ (Bothwell et al. 2010; Tacconi et al. 2008).

Конечно, есть детали, но уйти от эффективности 100% СЛОЖНО

While it is unlikely that any of these effects alone are able to explain the discrepancy, it is possible that invoking a few simultaneously could decrease the offset. Taking into consideration each of the caveats listed above, it is possible that the current observed tension with the local Kennicutt-Schmidt relation is not due to low-dust and increased star-formation efficiency, but a combination of bursty star-formation, top-heavy IMF, larger UV sizes, low covering fractions, or exceptionally high molecular gas content.